

Insulation Resistance Degradation in Ni–BaTiO₃ Multilayer Ceramic Capacitors

Donhang (David) Liu

Abstract—Insulation resistance (IR) degradation in Ni–BaTiO₃ multilayer ceramic capacitors has been characterized by the measurement of both time to failure (TTF) and direct current leakage as a function of stress time under highly accelerated life test conditions. The measured leakage current-time dependence data fit well to an exponential form, and a characteristic growth time τ_{SD} can be determined. A greater value of τ_{SD} represents a slower IR degradation process. Oxygen vacancy migration and localization at the grain boundary region results in the reduction of the Schottky barrier height and has been found to be the main reason for IR degradation in Ni–BaTiO₃ capacitors. The reduction of barrier height as a function of time follows an exponential relation of $\phi(t) = \phi(0)e^{-2Kt}$, where the degradation rate constant $K = K_0e^{(-E_k/kT)}$ is inversely proportional to the mean TTF (MTTF) and can be determined using an Arrhenius plot. For oxygen vacancy electromigration, a lower barrier height $\phi(0)$ will favor a slow IR degradation process, but a lower $\phi(0)$ will also promote electronic carrier conduction across the barrier and decrease the IR. As a result, a moderate barrier height $\phi(0)$ (and therefore a moderate IR value) with a longer MTTF (smaller degradation rate constant K) will result in a minimized IR degradation process and the most improved reliability in Ni–BaTiO₃ multilayer ceramic capacitors.

Index Terms—Barium titanate, ceramic capacitors, dielectric degradation, insulation resistance (IR), reliability.

I. INTRODUCTION

INSULATION resistance (IR) degradation related to oxygen vacancy migration has been considered to be the primary cause of reliability degradation of multilayer ceramic capacitors (MLCCs) with base-metal electrodes (BMEs). The behavior is characterized by a slow increase in the leakage current under an applied direct current (dc) field stress. To reveal IR degradation in a timely manner, MLCCs are often degraded under highly accelerated life test (HALT) conditions with different temperatures and applied voltages. Previous studies have shown that there are three possible factors related to the IR degradation of BaTiO₃-based BME MLCCs: the dielectric layer, the BaTiO₃ grain boundaries, and the Ni–BaTiO₃ internal electrode interfaces [1]–[4].

Unlike traditional BaTiO₃-based MLCCs with precious-metal electrodes (PMEs), BME MLCCs are cofired in a

reducing atmosphere to avoid oxidation of the electrodes. Despite the reoxidation process, there is still a significant amount of oxygen vacancies that are accommodated in the BaTiO₃ dielectric layers. The failure mechanism of BME MLCCs is thought to be dominated by the electromigration of oxygen vacancies through the grain boundaries in the dielectric layers [5]–[8]. Waser [9], Waser *et al.* [10], [11], and Baiatu *et al.* [12] studied the IR degradation in ambient-fired SrTiO₃ ceramic and acceptor-doped single-crystal SrTiO₃. The results showed that IR degradation begins with oxygen vacancy electromigration toward the cathode with respect to time, field, and temperature. Segregation of defects and dopants is found at the grain boundaries during the sintering process and results in the formation of space-charge layers at the grain boundaries.

The formation of double Schottky depletion layers at the grain boundaries of ceramic BaTiO₃ and their impact on the properties of BaTiO₃ ceramics was first proposed in [13] to explain the unique positive temperature coefficient of resistance (PTCR) behavior around the Curie temperature, which only existed in donor-doped semiconducting BaTiO₃ ceramics. This model indicates that the depletion barriers are formed because of the electron trapping by acceptor states at grain boundaries. Jonker [14], [15] later extended the Heywang model, considering the influence of ferroelectric polarization on resistivity below the Curie temperature.

In BaTiO₃-based MLCCs, the depletion layers are believed not only to be depleted of electron carriers and therefore to be highly resistive but also to act as electrical barriers against oxygen vacancy electromigration and, thus, to slow down the degradation process [2], [10], [16]. Although high-resistance depletion layers both at grain boundaries and at electrode interfaces limit electronic conduction and the transport of oxygen vacancies across dielectric layers, oxygen vacancy migration is either trapped near the grain boundary depletion layers or blocked by electrode interfaces, and these charged oxygen vacancies are neutralized by the reduction of Ti⁴⁺ near the cathode and the rare-earth (RE) doping in the BaTiO₃ dielectric. This agrees with a number of recently published works about first-principles calculations of RE element doping, the local atomic configuration, and the solution energy of oxygen vacancies [17]–[19].

In this paper, the IR degradation in Ni–BaTiO₃ MLCCs was investigated for three commercial BME capacitors qualified to the same reliability level but made by different manufacturers. This paper provides insight into the time-dependent correlations among oxygen vacancy migration, vacancy trapping,

Manuscript received December 5, 2013; revised July 11, 2014; accepted November 7, 2014. Recommended for publication by Associate Editor F. G. Canavero upon evaluation of reviewers' comments.

The author is with the ASRC Federal Space and Defense, NASA Goddard Space Flight Center, Greenbelt, MD 20771 USA (e-mail: donhang.liu-1@NASA.gov).

Color versions of one or more of the figures in this paper are available online at <http://ieeexplore.ieee.org>.

Digital Object Identifier 10.1109/TCPMT.2014.2374576

TABLE I
SPECIFICATIONS AND CALCULATED E (kV/mm), AND VOLTS PER GRAIN (V/GRAIN)

Part ID	Stress Level	E (kV/mm)	V/Grain
AA46450 0.47 μ F, 50V, 0805 Manufacturer A 98 layers BaTiO ₃ thickness= 6.39 μ m Ave. grain size= 0.38 μ m	250V 175C	39.1236	14.75
	225V 165C	35.2113	13.27
	250V 165C	39.1236	14.75
	250V 155C	39.1236	14.75
	315V 155C	49.2958	18.59
AB47450 0.47 μ F, 50V, 0805 Manufacturer B 100 layers BaTiO ₃ thickness= 5.80 μ m Ave. grain size= 0.33 μ m	250V 175C	43.0886	14.13
	225V 165C	38.7797	12.72
	250V 165C	43.0886	14.13
	250V 155C	43.0886	14.13
	315V 155C	54.2916	17.81
AC47450 0.47 μ F, 50V, 0805 Manufacturer C 103 layers BaTiO ₃ thickness= 8.10 μ m Ave. grain size= 0.40 μ m	250V 175C	30.8642	12.45
	225V 165C	27.7778	11.20
	250V 165C	30.8642	12.45
	250V 155C	30.8642	12.45
	315V 155C	38.8889	15.68

and the depletion layer height. A theoretical model based on the oxygen vacancy migration and entrapment at grain boundary is proposed to show the relationship between the reliability, characterized by mean time to failure (MTTF), and the depletion layer height reduction during the IR degradation in the BaTiO₃ dielectric materials of BME capacitors.

II. EXPERIMENTAL PROCEDURE

Three automotive-grade commercial BME capacitors, AA47450, AB47450, and AC47450, with the same chip size, capacitance, and rated voltage, but made by different manufacturers, were selected for this paper. These BME capacitors were qualified per AEC-Q200, a specification document developed by the Automotive Electronics Council of United States for ceramic capacitors and passive components used in harsh automotive environments. The microstructures of the three BME capacitor lots were investigated by cross section processing of five units per capacitor type and were examined using a scanning electron microscope to reveal the number of dielectric layers, average grain size, and average dielectric layer thickness.

Table I summarizes the specifications, number of dielectric layers, corresponding electrical field (V/thickness), and volts per grain at a given stress condition used to degrade the capacitors to reveal their failure modes. The electric field can be calculated by dividing the measured dielectric thickness by the applied voltage. The volts per grain (the voltage applied to each individual BaTiO₃ grain) can be calculated using the dielectric thickness and measured average grain size data from the microstructure analysis.

The results in Table I show that at a given applied voltage, the values of volts per grain are very similar among the three BME capacitor lots, indicating that these capacitors are not only manufactured and qualified to the same reliability level but they will also have a similar applied electrical strength during degradation. The three BME capacitor lots were degraded together under the same HALT temperature and applied voltage conditions, as shown in Table I. Twenty BME capacitors

were tested for each stress condition and for each capacitor type.

The traditional HALT measures only the time-to-failure (TTF) data of each capacitor at a given stress condition, and then uses a statistical model to determine the MTTF data at this stress condition [19]–[22]. This approach is based on a single failure mode assumption and is adequate for most ceramic capacitors with precious-metal electrodes (PMEs). However, as has been previously shown [26]–[29], many BME capacitors, when degraded under HALT conditions, reveal a more complicated failure mechanism with two distinct failure modes. A recently performed failure analysis of these degraded BME capacitors also confirms the existence of two distinct failure modes [37]. For this reason, the measurement of TTF data alone will not result in an accurate prediction of the reliability life of these BME capacitors. To characterize the multiple failure modes in BME capacitors, the leakage current was also monitored *in situ* and was measured every 1–3 s for each capacitor unit. The reliability life of a capacitor is, thus, not only determined by the TTF data but also by the measured leakage current data used to distinguish the failure modes. To differentiate this new approach from the traditional single-failure mode HALT that measures TTF data only, this modified method that has been used with multiple failure modes has been dubbed highly accelerated life stress testing (HALST) [29]. The term HALST is used through the remainder of this paper as appropriate.

When IR degradation is accelerated under HALST conditions, a certain value of IR or of leakage current must be used as the failure criterion at which the TTF can be determined. Per MIL-PRF-123, BaTiO₃-based MLCCs built for high-reliability applications were constructed with a minimum dielectric thickness of 25 μ m for rated voltages greater than 50 V. In this case, the leakage current level was very low, even under HALST conditions. The MLCC was considered a failure when IR at a given stress condition was degraded three to four orders below its initial value [20], [21]. Waser *et al.* [10] have also defined characteristic lifetime t_{ch} at which the leakage

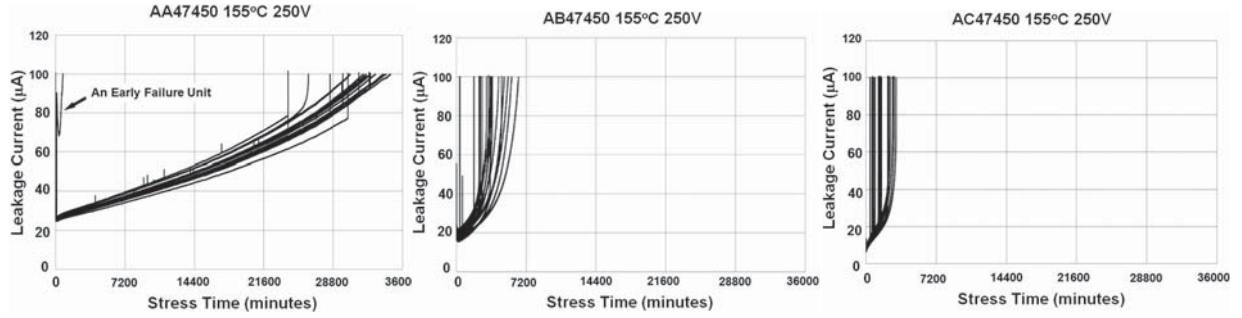


Fig. 1. Leakage current as a function of stress time for the three BME capacitor lots, degraded at 155 °C, 250 V. The plots were made with the same x -axis scale to reveal the difference in TTF data.

current has risen one decade above its minimum value to evaluate the degradation rate. With the progress in Ni-BaTiO₃ MLCC development, dielectric thicknesses have been significantly reduced, even below 2 μm [22]. As a result, leakage current has increased significantly, and Ni-BaTiO₃ MLCCs are considered to have failed at a fairly low IR value. Some reports define the TTF as the time at which IR is degraded to a value of 500 k Ω [22], [23], 1000 k Ω [24], or 10% of its initial value [4], while others set a constant leakage current limit at 100 μA for all of the stress conditions being used [25]–[29]. After a review of most of the failure criteria that have been reported for determining the TTF of MLCCs with BaTiO₃ dielectrics, the author decided to use a single current limit of 100 μA to determine the TTF for all stress levels and for all MLCC samples, based on the following considerations.

During HALST, each MLCC unit was connected in series to a current-limiting resistor with a dc power supply. The voltage drop across the series resistor was measured and used to calculate the leakage current of the capacitor. Since the voltage drop on the current-limiting resistor is dependent on the current value, a leakage current higher than 100 μA can result in a voltage drop on the current-limiting resistor of more than 5% of the overall applied voltage. This is true for a number of BME capacitors with thin dielectric layers that can be degraded under fairly low applied voltages. Although this voltage drop can be reduced if a smaller value resistor is used, the voltage value reading on a small resistor may be too low to ensure the accuracy of the IR measurement. For example, when an MLCC with a 100 k Ω resistor is accelerated at 150 V, the voltage drop will be 100 k Ω \cdot 100 μA = 10 V, which is 6.7% of the total applied voltage. For a 1 k Ω resistor, the voltage drop is only 0.1 V across the resistor, which may be too low to show the details of the leakage current changing with the stress time. In this paper, the values of the resistor were chosen such that the maximum voltage drop at the current-limiting resistor will be no more than 3% of the applied voltage under all HALST conditions.

III. RESULTS AND DISCUSSION

A. Characterization of Time-Dependent Leakage Current and MTTF Data

1) *Leakage Current and MTTF Data*: Fig. 1 shows the leakage current against stress time for the three BME capacitor lots at a given stress condition: 155 °C, 250 V (5 \times rated voltage).

TABLE II
MTTF DATA OF THE THREE BME CAPACITOR LOTS
AT VARIOUS STRESS CONDITIONS

Test Conditions	MTTF (Minutes) of BME Capacitors		
	AA47450	AB47450	AC47450
250V 175C	1466	450	319
250V 165C	9869	1140	626
225V 165C	15423	2066	1046
250V 155C	31602	3659	1479
250V, 145C	86400	8895	2458
315V 155C	17721	1102	648

The plots in Fig. 1 have the same scale on the x -axis. It can be seen that these capacitor lots, when degraded at the same stress condition, revealed significantly different TTF data. Further details about the characterization of the failure patterns and about the method to determine the acceleration factors have been discussed in [29].

A two-parameter Weibull plot can be made when TTF data at a given stress level are available. The MTTF, a statistical parameter that measures reliability, can be determined as

$$\text{MTTF} = \eta \Gamma(1 + \beta^{-1}) \quad (1)$$

where slope β is the dimensionless shape parameter whose value is often characteristic of the particular failure mode, η is the scale parameter that represents the time at which 63.2% of the population has failed, and $\Gamma(x)$ is the gamma function of x .

Table II summarizes the calculated MTTF data using (1) when all TTF data at a given stress level were used to make a two-parameter Weibull plot. The reliability life, as characterized by MTTF, was more than one magnitude of difference among the capacitor lots under the same stress condition.

2) *Characterization of Leakage Current Data for a Slow Degradation Failure Mode*: As shown in Table I, all three BME capacitor lots that were made for the same reliability level revealed almost identical construction and microstructure parameters and were also degraded under very similar stress conditions. However, the MTTF data contained in Table II show significant differences in reliability life for these BME capacitors. To understand the mechanism that determines the reliability life, the leakage current data shown in Fig. 1 were replotted with a different scale in the x -axis to reveal

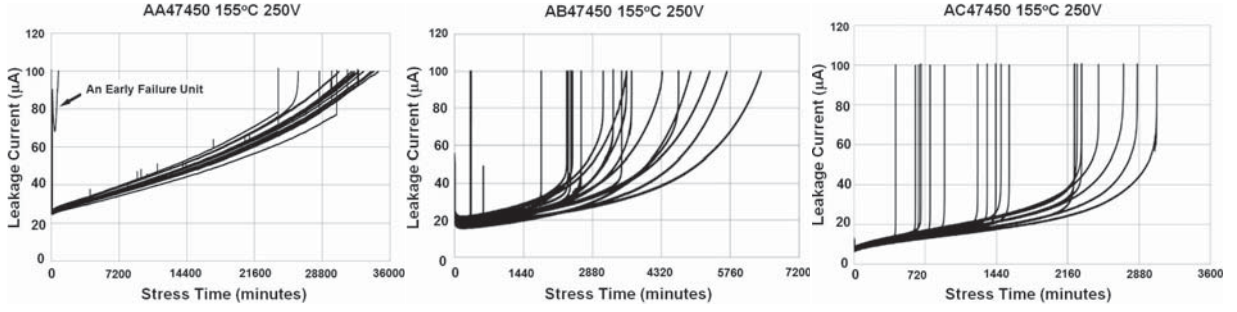


Fig. 2. Leakage data are replotted from Fig. 1 with a different scale in the x -axis to reveal details in the failure modes among the three BME capacitor lots.

details of the differences in their failure modes. As shown in Fig. 2, the TTF data appear to be highly dependent on the failure mode exhibited during the HALST regimen.

As discussed in [27]–[29], two failure modes can be identified in these BME capacitor lots: catastrophic and slow degradation. A catastrophic failure is characterized by a time-accelerating increase in leakage current that is mainly due to existing processing defects (voids, cracks, delaminations, and so on) or to extrinsic defects. A slow degradation failure is characterized by a near-linear increase in leakage current against stress time; this is caused by the electromigration of oxygen vacancies (intrinsic defects). The TTF data shown in Fig. 2 clearly indicate that BME capacitors with slow degradation failures exhibit the largest MTTF values (AA47450), and those with the most catastrophic failures showed the smallest MTTF values (AC47450). Capacitor lot AB47450 shows failures with both failure modes and with MTTF values in between those of the other two capacitor lots.

As shown in Fig. 2, for a certain period of stress time, the leakage current follows a slow degradation failure mode, i.e., a gradual increase in leakage current against stress time. With a further increase of stress time, some capacitors will fail catastrophically, while some will retain the slow degradation failure mode until the failure criterion is reached.

The leakage data shown in Fig. 2 have been curved-fitted with a number of different mathematical functions (power law, exponential, linear, logarithmic, and so on). Although the leakage data shown in Fig. 2 appear to be linear against most of the stress time measured, the curve-fitting results have shown that the exponential form of

$$I = I(t_0)e^{\left(\frac{t-t_0}{\tau_{SD}}\right)} \quad (2)$$

fits the leakage data better than a linear form. In (2), I is the measured leakage current, $I(t_0)$ is the leakage value at $t = t_0$, and τ_{SD} is a characteristic exponential growth time.

Fig. 3 shows an example of curve fitting using (2) for two capacitor samples with different failure modes. C13, with a near-linear increase in leakage, fits very well to (2) when all of the measured leakage data points and a method of least squares were used. Although C7 fails with a catastrophic failure characterized by a rapid leakage current increase at the end, the majority of the leakage data follow a slow degradation failure mode and still fit well to (2). A similar value of τ_{SD} to that of C13 could be obtained. For some of the leakage

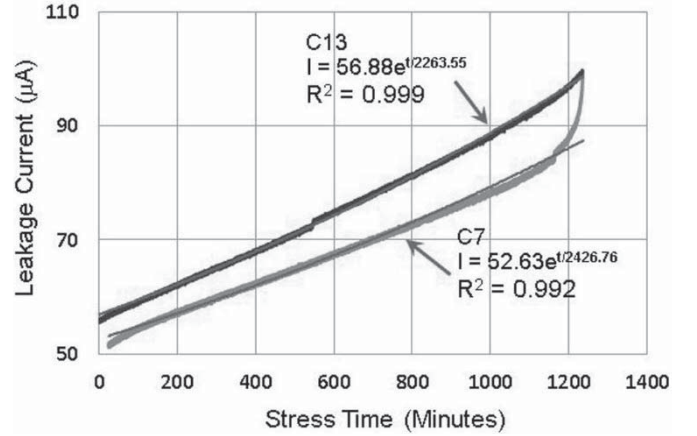


Fig. 3. Examples of curve fitting using (2) for two BME capacitor samples with different failure patterns. Both appear to fit well to the exponential form of (2) for most of the stress time.

data that finished with a strong catastrophic failure, to obtain a proper value of τ_{SD} , some of the leakage data points at the catastrophic failure side have to be gradually removed until a value of $R^2 \geq 0.99$ is reached.

The meaning of τ_{SD} can be illustrated by the following example: let I_1 and I_2 be the leakages at t_1 and t_2 , respectively, for a slow degradation failure. If one assumes $(I_2/I_1) = 2$, then (2) can be rewritten as

$$\frac{I_2}{I_1} = e^{\left(\frac{t_2-t_1}{\tau_{SD}}\right)} = e^{\left(\frac{\Delta t}{\tau_{SD}}\right)} = 2$$

and

$$\tau_{SD} = \frac{\Delta t}{\ln(2)} \approx 1.4427 \cdot \Delta t \quad (3)$$

where Δt is the time at which the leakage current doubles in value. The greater the value of τ_{SD} , the longer the timespan of a degradation failure, indicating a slower IR degradation process.

At a given stress condition, when the τ_{SD} of all 20 BME capacitors being tested was obtained using the curve-fitting method described above, a two-parameter Weibull plot could be made, and an average value of τ_{SD} , $\langle \tau_{SD} \rangle$, was defined as the scale parameter η of the Weibull plot.

Table III summarizes the values of $\langle \tau_{SD} \rangle$ determined for various stress conditions. The table can be used to compare the corresponding MTTF data. In most cases, the value

TABLE III
CALCULATED MTTF DATA FROM WEIBULL PLOTS OF TTF DATA AND
CALCULATED $\langle\tau_{SD}\rangle$ FROM THE CURVE-FITTING OF THE THREE BME
CAPACITOR LOTS AT THREE DEGRADATION CONDITIONS

	MTTF (Minutes)	$\langle\tau_{SD}\rangle$ (Minutes)
Test Conditions	AA47450	
250V, 175°C	1466	3333
250V, 165°C	9869	11111
250V, 155°C	31602	34925
Test Conditions	AB47450	
250V, 175°C	450	667
250V, 165°C	1140	1714
250V, 155°C	3659	3333
Test Conditions	AC47450	
250V, 175°C	319	357
250V, 165°C	626	769
250V, 155°C	1479	1667

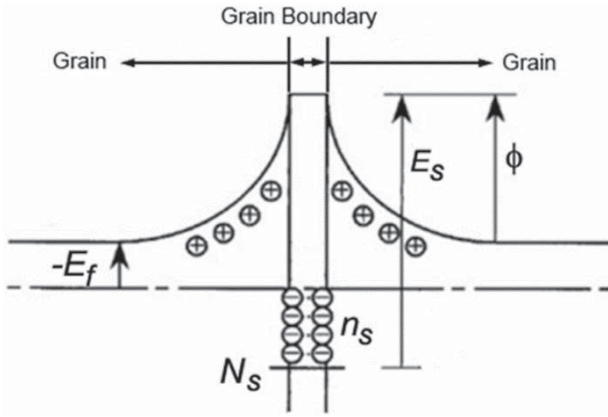


Fig. 4. Schematic of the formation of a double Schottky barrier around the grain boundary of a BaTiO₃ ceramic capacitor, where ϕ is the depletion barrier height; n_s is the concentration of trapped electrons at the grain boundary surface acceptor states whose number is N_s (cm⁻²); and E_s is the energy level of the surface states from the conduction level of the bulk.

of $\langle\tau_{SD}\rangle$ was greater than that of MTTF, but it was smaller in a few lower-stress levels where the catastrophic failure mode is dominant. Certainly, the relationship between TTF and τ_{SD} depends upon the failure criterion, and if a fixed absolute value of leakage current is selected as the failure criterion, then the relationship depends on the value chosen and on the initial leakage current value for the capacitors.

B. IR Degradation Model for BME Capacitors

1) *Time-Dependent Depletion Layer Height $\phi(t)$* : Although the formation of a double Schottky barrier layer at a grain boundary, as shown in Fig. 4, was initially proposed to explain the PTCR effect in donor-doped semiconducting BaTiO₃ ceramics [13]–[15], the same barrier depletion layer model has also been suggested to explain the IR degradation in Ni-BaTiO₃ MLCCs [2], [4], [9]–[11]. The typical barrier height can be expressed as

$$\phi = \frac{e^2 N_d d^2}{2\epsilon_0 \epsilon_r}$$

where N_d is the donor concentration, d is the depletion layer thickness, e is the electron charge, and $\epsilon_0 \epsilon_r$ is the dielectric constant. The electroneutrality condition in the depletion layer satisfies the following requirement [13]:

$$d = \frac{n_s}{2N_d} \quad (4)$$

where n_s is the concentration of trapped electrons at grain boundary surface acceptor states (the number is N_s) (cm⁻²). The barrier height ϕ can be rewritten as

$$\phi = \frac{e^2 n_s^2}{8\epsilon_0 \epsilon_r N_d} \quad (5)$$

Equation (5) has often been used to estimate the grain boundary barrier height in semiconducting BaTiO₃ ceramics [34], [38]. In Ni-BaTiO₃ MLCCs, N_d is mainly determined by the bulk concentration of ionized oxygen vacancies. Although oxygen vacancies migrate under an applied dc field and the weakly bonded electrons can be trapped by the surface acceptor states, the value of depletion layer thickness d in (4) is always in the submicrometer range, indicating that $N_d \gg n_s$. Therefore, one can assume that $N_d(t) \approx N_d(0)$, and one can also assume time independence. Therefore, the time-dependent barrier height ϕ can be expressed as

$$\frac{d\phi(t)}{dt} = \frac{d}{dt} \left(\frac{e^2 n_s^2}{8\epsilon_0 \epsilon_r N_d} \right) = \frac{e^2}{4\epsilon_0 \epsilon_r N_d} \frac{dn_s(t)}{dt}$$

To determine $dn_s(t)/dt$, the following facts were considered.

- 1) $n_s(t)$ is trapped electrons at surface acceptor states in the grain boundary regions. The negative space charge due to trapped electrons is compensated for by the formation of a positive space charge region near the grain boundary, which behaves like a depletion barrier layer to electron conduction.
- 2) The computational analysis on the trapping of oxygen vacancies at grain boundaries with respect to local atomic configuration and energy shows that grain boundaries attract oxygen vacancies and trap them at specific sites at which local cation density is lower than that in the grain interior [17].
- 3) Since oxygen vacancies behave like donors, they possess positive space charges when ionized. The same positive space charge in a barrier layer at a grain boundary will thus act as a resistance for positively charged oxygen vacancy diffusion in a polycrystalline BaTiO₃ dielectric. As a result, when an ionized oxygen vacancy migrates under a dc field and reaches the barrier layer, it has a tendency to become trapped there. The electroneutrality condition requires that the weakly bonded two electrons that are moving in a conduction band now have to be localized to make the trapped oxygen vacancy neutralize and to become part of the crystalline structure.

When Kröger and Vink [31] symbols are used, the process can be described by

$$V_O = V_O^{\bullet\bullet} + 2e' \quad (6)$$

As reported in [4], the localized electrons that compensate the $V_O^{\bullet\bullet}$ localization can be trapped with the reduction of

Ti ions surrounding the $V_O^{\bullet\bullet}$ as $Ti^{4+} + e' \rightarrow Ti^{3+}$, and $Ti^{3+} + e' \rightarrow Ti^{2+}$ [4]. The reduction of Ti^{4+} will now reduce the positive space charge in the positively charged depletion layer and reduce the barrier height. Since the barrier height is balanced by the trapped electrons in surface acceptor states $n_s(t)$, the reduction in barrier height will lower the Fermi level at grain boundary, and then will reduce the $n_s(t)$. If we assume that Δn_O is the electron concentration that has been localized to make the trapped $V_O^{\bullet\bullet}$ neutral, Δn_O should meet the following conditions: at $t = 0$, $\Delta n_O(0) = 0$, and at $t \rightarrow \infty$, $\Delta n_O = n_s(0)$, i.e., all trapped electrons at $t = 0$ in the surface acceptor states $n_s(0)$ will eventually be fully compensated for by the localized electrons that neutralize the trapped $V_O^{\bullet\bullet}$. However, with a further increase of Δn_O as more $V_O^{\bullet\bullet}$ are trapped and neutralized, the electrically negative feature of $n_s(t)$ will further retard the localization of electrons and reduce the localization rate of Δn_O . Therefore, the change of Δn_O as a function of t can be expressed by a first-order reaction according to the reaction rate theory [30]

$$\frac{d\Delta n_O(t)}{dt} = K(t)[n_s(0) - \Delta n_O(t)]$$

and

$$\int_{\Delta n_O(0)}^{\Delta n_O(t)} \frac{d\Delta n_O(t)}{\Delta n_O(t) - n_s(0)} = \int_0^t -K(t)dt \quad (7)$$

where $K(t)$ is the degradation rate constant and $n_s(0) - \Delta n_O(t) = n_s(t)$ is the trapped electron concentration at surface acceptor states at time t . If $\Delta n_O(t)$ is only balanced by $n_s(t)$ near the Fermi level, $K(t) = K = K_0 e^{-E_k/kT}$ can be simplified as a time-independent constant in which E_k is the activation energy that is required for $V_O^{\bullet\bullet}$ in electromigration to be neutralized at a grain boundary region per (6) and k is the Boltzmann constant. Since $\Delta n_O(0) = 0$, (7) finally yields

$$\frac{n_s(0) - \Delta n_O(t)}{n_s(0)} = e^{-Kt}$$

and

$$\Delta n_O(t) = n_s(0)(1 - e^{-Kt}) \quad (8)$$

the remaining trapped electrons in acceptor states can be simply expressed according to (8) as

$$n_s(0) - \Delta n_O(t) = n_s(0) - n_s(0)(1 - e^{-Kt}) = n_s(0)e^{-Kt}.$$

Combining (5) and (8) yields a time-dependent barrier height

$$\phi(t) = \frac{e^2[n_s(0) - \Delta n_O(t)]^2}{8\epsilon_0\epsilon_r N_d} = \phi(0)e^{-2Kt}. \quad (9)$$

This relationship indicates that the barrier height will exponentially decrease with time due to the oxygen vacancy entrapment at grain boundaries.

2) *Determination of Degradation Rate Constant K*: The measurement of I - V characteristics of ceramic BaTiO₃ inside the grain interior and at the grain boundary has shown that under an applied field of 100 kV/cm, the current density inside the grain and at the grain boundary can differ by several orders of magnitude. The difference increases significantly as temperature increases [33]. It is the grain boundary that

holds the high resistivity of the ceramic BaTiO₃. If all grain boundaries inside a dielectric layer are assumed to have a uniform barrier height $\phi(t)$, the time-dependent resistivity $\rho(t)$ of an MLCC can be written as [13]

$$\rho(t) = \rho_0 e^{\left(\frac{\phi(t)}{kT}\right)} \quad (10)$$

where ρ_0 is the resistivity of the grain interior. According to (2), the time-dependent current density of an MLCC $j(t)$ for a slow degradation failure mode can be expressed as

$$j(t) = j(t_0)e^{\left(\frac{t-t_0}{\tau_{SD}}\right)} = \frac{E}{\rho(t)}$$

or

$$\rho(t) = \frac{E}{j(t_0)} e^{-\left(\frac{t-t_0}{\tau_{SD}}\right)} \quad (11)$$

where $j(t_0)$ is the current density at $t = t_0$ and E is the applied field. Combining (10) and (11) results in

$$\begin{aligned} \rho(t) &= \rho_0 \exp\left(\frac{\phi(t)}{kT}\right) = \rho_0 \exp\left(\frac{\phi(0)e^{-2Kt}}{kT}\right) \\ &= \frac{E}{j(t_0)} \exp\left(-\frac{t-t_0}{\tau_{SD}}\right). \end{aligned}$$

At a given stress level, E is a constant, so

$$\frac{t-t_0}{\tau_{SD}} \approx -\frac{\phi(0)}{kT} e^{-2Kt}. \quad (12)$$

Using $\langle\tau_{SD}\rangle$, the average of τ_{SD} , to replace τ_{SD} , and $e^{-x} \approx 1 - x$ when x is small, the integration of (12) results in

$$\begin{aligned} \int_0^{\text{MTTF}} \frac{t-t_0}{\langle\tau_{SD}\rangle} dt &= -\int_0^{\text{MTTF}} \frac{\phi(0)}{kT} \cdot e^{-2Kt} dt \\ &\approx -\int_0^{\text{MTTF}} \frac{\phi(0)}{kT} (1 - 2Kt) dt \end{aligned}$$

and

$$\frac{1}{2\langle\tau_{SD}\rangle} \approx \frac{\phi(0)}{kT} \left(K - \frac{1}{\text{MTTF}} \right).$$

This gives rise to

$$\frac{1}{\text{MTTF}} = K - \frac{kT}{2\phi(0)\langle\tau_{SD}\rangle} \approx K_0 e^{-\frac{E_k}{kT}}. \quad (13)$$

Equation (13) is the well-known Prokopowicz-Vaskas equation for MLCCs, when applied voltage is a constant [35]. The degradation rate constant K can now be determined by an Arrhenius plot using the MTTF data obtained at various temperatures and at a constant voltage.

Using the MTTF data at different temperatures and at a given voltage (250 V) for the three BME capacitor lots, a corresponding Arrhenius plot according to (13) can be plotted, as shown in Fig. 5. Both activation energy E_k and degradation rate constant K_0 can now be determined.

Table IV lists the activation energy E_k and constant K_0 at three different temperatures for the three BME capacitor lots. The calculated K values shown in Table IV were used to estimate the MTTF data per (13). A comparison between the measured MTTF data and the calculated data shows fairly good agreement. All calculated MTTF values are smaller than the measured ones. For lot AA47450, the MTTF data

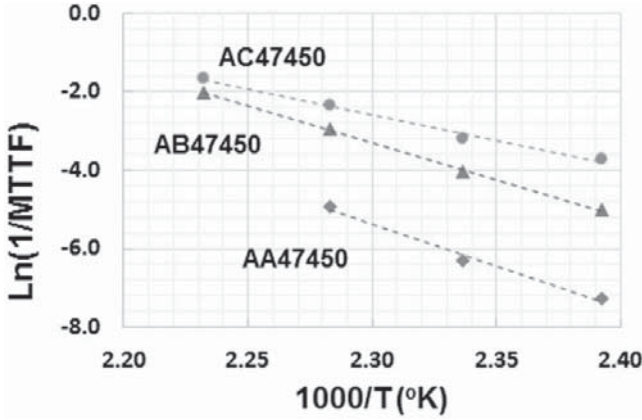


Fig. 5. Arrhenius plots using (13) and measured MTTF data in Table II for the three BME capacitor lots.

measured at 175 °C were excluded for the estimation of the degradation rate constant K because its value is much smaller when combined with other MTTF data points to give rise to a good linear fitting. Since the BME capacitor lot under degradation was so leaky at this temperature, the results of self-heating due to the leakage current could result in a significant amount of temperature increase, and thus an acceleration in the failure of the BME capacitors.

C. IR Degradation Mechanism Due to Oxygen Vacancy Electromigration

1) *Reliability and Oxygen Vacancy Migration*: According to (9)

$$\phi(t) = \phi(0)e^{-2Kt} = \phi(0)e^{-\frac{2t}{\text{MTTF}}}$$

and

$$\frac{1}{\text{MTTF}} = \approx K_0 e^{-\frac{E_k}{kT}}$$

where $K = K_0 e^{(-E_k/kT)}$ is the degradation rate constant for oxygen vacancy entrapment at grain boundaries. Although K and MTTF can be related to each other per the Prokopowicz–Vaskas equation, the physical meaning of K was clearly defined in the proposed model. To make Ni-BaTiO₃ BME capacitors with improved reliability, the value of K must be minimized. This requires a smaller value of the degradation constant K_0 , which is the total number of oxygen vacancies that are migrateable; and a large value of E_k , which is the activation energy required for $V_{\text{O}}^{\bullet\bullet}$ to be neutralized and trapped near the depletion layer at grain boundaries. This has been proven from the calculated K values shown in Table IV, where AA47450 and AB47450 are shown to have similar values of E_k but a much smaller value for K_0 , which gives rise to a significantly improved reliability life (larger MTTF) for capacitor AA47450.

On the other hand, since a typical barrier height value of $\phi(0) \approx 1.30$ eV has been reported in [4], a large value of $E_k > \phi(0)$ is necessary to slow down the $V_{\text{O}}^{\bullet\bullet}$ entrapment, because a large value of E_k also means that the entrapment of $V_{\text{O}}^{\bullet\bullet}$ at grain boundaries may not be an energetically favorable

process unless the barrier height $\phi(t)$ is high enough to be comparable to E_k . This is the case for AC47450, where $E_k = 1.11$ eV is smaller than that of $\phi(0)$. Therefore, the oxygen vacancies are more energetically favorable for local entrapment than for migrating across the depletion barrier, and they result in a very small reliability life when compared with the other two BME capacitor lots.

Finally, since $N_d \gg n_s$ per (4), only a tiny fraction of oxygen vacancies can be trapped at the grain boundaries during the electromigration across the dielectric layer to cause IR degradation. This indicates that the effort to simply reduce the level of $V_{\text{O}}^{\bullet\bullet}$ in the dielectric material would not significantly slow down the IR degradation. Indeed, a small value of K_0 indicates that the number of electromigrateable $V_{\text{O}}^{\bullet\bullet}$ must be minimized. The recent first-principles calculations based on the density function theory have shown that some kinds of dopants in BaTiO₃ dielectrics, such as RE and alkaline-earth (AE) elements, were effective in improving the reliability life of Ni-BaTiO₃ capacitors [17]–[19]. According to the IR degradation model proposed here, both RE and AE doping would benefit from the frozen migrateable $V_{\text{O}}^{\bullet\bullet}$, and thus reduce the value of K_0 . On the other hand, some RE doping elements, such as Dy and Er, due to their amphoteric characteristics, will also benefit from the formation of deep surface acceptable states N_S to result in a large value of E_k . The correlations between the formulation and the value of the degradation rate constant for oxygen vacancy entrapment K as defined in this paper needs to be further investigated.

2) *Insulation Resistance and Reliability Life*: According to (12)

$$e^{\frac{t-t_0}{\tau_{\text{SD}}}} \approx e^{-\frac{\phi(0)}{kT}} e^{-2Kt}$$

which indicates that a slower IR degradation process, characterized by a larger value of τ_{SD} , would give rise to a smaller value of $\phi(0)$. This makes sense since a smaller $\phi(0)$ will energetically be favorable to the continuous electromigration of $V_{\text{O}}^{\bullet\bullet}$ without being trapped at a grain boundary to cause an IR degradation. However, this is only one part of the equation; $\phi(0)$ also presents the barrier height for the conduction band electronic carriers. A lower $\phi(0)$ will facilitate electronic conduction and will also deteriorate the IR. As a result, when electron conduction and oxygen vacancy electromigration are both considered, a moderate initial barrier height $\phi(0)$ and a smaller K are the keys for slowing the IR degradation in Ni-BaTiO₃-based ceramic capacitors, and thus improving their reliability life.

As an important conclusion of this model development, higher IR values may not always result in a larger MTTF, but a slower IR degradation rate (smaller K) will always have this effect. This conclusion can be verified from the measured leakage data shown in Fig. 3, where sample AC47450 was shown to have the highest initial IR values and smallest MTTF and AA47450 had the lowest initial IR values but the largest MTTF among the group.

A higher $\phi(0)$ generally means a higher resistance, and therefore a higher electrical strength when a dc voltage is applied. A higher dc electrical strength makes it more likely

TABLE IV
CALCULATED DEGRADATION CONSTANT K AND MTTF DATA PER THE CURVE-FITTING RESULTS IN FIG. 5 AND (13)

Capacitor ID	E_k (eV)	$K_0 e^{-\frac{E_k}{kT}}$ (hour ⁻¹)		MTTF (minutes) at 155°C, 250V	
		at 398K (125°C)	at 428K (155°C)	Measured	Calculated
AA47450	1.65	7.38×10^{-5}	2.10×10^{-3}	31602	28640
AB47450	1.63	6.76×10^{-4}	1.86×10^{-2}	3459	3218
AC47450	1.11	4.94×10^{-3}	4.73×10^{-2}	1479	1268

that a thermal-related electrical breakdown will be experienced due to the localization of the electrical strength [9]–[11].

3) *Oxygen Vacancy Migration and Compensation*: Since only a very small portion of $V_{O}^{\bullet\bullet}$ may be trapped at the grain boundaries, the majority of $V_{O}^{\bullet\bullet}$ will continually migrate and will eventually reach the dielectric layer and internal Ni electrode interface, as has been shown by previously reported electron energy loss spectroscopy and high-resolution transmission electron microscope observations [4].

Since there is no evidence to show that $V_{O}^{\bullet\bullet}$ can be transferred across the cathode electrode layer [4], [10] most $V_{O}^{\bullet\bullet}$ capable of migration will now pile up along the Ni-electrode dielectric interface. To neutralize these vacancies, a significant number of electrons is required, which can only be obtained from the cathode electron injection. The energy required for cathode electron injection at the dielectric-electrode interface is ~ 1.25 eV [36]. If E_k is less than this, most of the oxygen vacancies will be energetically favorable for localization, and a quick IR degradation will occur. This is exactly the case for lot AC47450.

The high concentration of localized electrons due to the compensation of the pile-up of oxygen vacancies will not only dramatically change the local stoichiometry of the BaTiO₃ dielectric but it will also lead to a leakage current increase during IR degradation. This will cause a local temperature increase and will eventually lead to the breakdown at the Ni–BaTiO₃ interface. The initial failure site of the dielectric-electrode interface was clearly revealed in a previously published failure analysis work regarding Ni–BaTiO₃ ceramic capacitors [37].

IV. CONCLUSION

Three BME capacitor lots with the same specification (chip size, capacitance, and rated voltage) and reliability level, made by three different manufacturers, were selected for reliability performance evaluation. The microstructure analysis of these capacitors showed that the three BME products had a similar number of dielectric layers and a similar number of grains per dielectric layer. When an external voltage was applied, the volts per grain was almost identical for these capacitors, indicating that the dielectrics will experience the same voltage stress when electrically tested under the same externally applied voltages.

These BME capacitors were then degraded using HALST under the same temperature and applied voltage conditions. The reliability life, as characterized by MTTF, differed by more than one order of magnitude among the capacitor lots.

A model based on the existence of depletion layers at grain boundaries and on the entrapment of electromigrateable oxygen vacancies was proposed to explain the MTTF difference among these BME capacitors. The MTTF has been found to be directly related to the degradation rate constant K of oxygen vacancy entrapment at grain boundaries. The MTTF and K were found to follow the traditional Prokopowicz–Vaskas equation at a constant applied voltage.

A lower depletion layer height $\phi(0)$ is energetically favorable for a slower degradation rate and a longer reliability life. However, when both oxygen vacancy migration and electronic conduction are considered, a $\phi(0)$ with a moderate height would give rise to the best reliability performance.

It is the conclusion of this paper that reliability will not be improved simply by increasing the IR. Indeed, Ni–BaTiO₃ BME capacitors with a smaller IR degradation rate constant K , or a smaller amount of entrapped $V_{O}^{\bullet\bullet}$ at grain boundaries, will always give rise to a longer reliability life.

Both RE and AE doping may have profound impacts on the values of degradation rate constant K , and the impacts needs to be further investigated.

ACKNOWLEDGMENT

The author appreciates NASA Electronic Parts and Packaging Program’s support for this paper. The author would like to thank NASA Goddard Space Flight Center Code 562 Parts Analysis Laboratory for assistance with electrical testing.

REFERENCES

- [1] H. Kishi, Y. Mizuno, and H. Chazono, “Base-metal electrode-multilayer ceramic capacitors: Past, present and future perspectives,” *Jpn. J. Appl. Phys.*, vol. 42, no. 1, pp. 1–15, Jan. 2003.
- [2] H. Chazono and H. Kishi, “DC-electrical degradation of the BT-based material for multilayer ceramic capacitor with Ni internal electrode: Impedance analysis and microstructure,” *Jpn. J. Appl. Phys.*, vol. 40, no. 9B, pp. 5624–5629, Sep. 2001.
- [3] G. Y. Yang *et al.*, “Oxygen nonstoichiometry and dielectric evolution of BaTiO₃. Part I—Improvement of insulation resistance with reoxidation,” *J. Appl. Phys.*, vol. 96, no. 12, pp. 7492–7499, Dec. 2004.
- [4] G. Y. Yang *et al.*, “Oxygen nonstoichiometry and dielectric evolution of BaTiO₃. Part II—Insulation resistance degradation under applied DC bias,” *J. Appl. Phys.*, vol. 96, no. 12, pp. 7500–7508, Dec. 2004.
- [5] K. Morita, Y. Mizuno, H. Chazono, and H. Kishi, “Effect of Mn addition on DC-electrical degradation of multilayer ceramic capacitor with Ni internal electrode,” *Jpn. J. Appl. Phys.*, vol. 41, no. 11B, pp. 6957–6961, Nov. 2002.
- [6] H. Chazono and H. Kishi, “Effect of Ho amount on microstructure and electrical properties of Ni-MLCC,” *Key engineering materials*, vol. 248, pp. 183–186, Aug. 2003.
- [7] D. F. K. Hennings, “Dielectric materials for sintering in reducing atmospheres,” *J. Eur. Ceram. Soc.*, vol. 21, nos. 10–11, pp. 1637–1642, Nov. 2001.

- [8] K. Albertsen, D. Hennings, and D. Steigelmann, "Donor-acceptor charge complex formation in barium titanate ceramics: Role of firing atmosphere," *J. Electroceram.*, vol. 2, no. 3, pp. 193–198, Nov. 1998.
- [9] R. M. Waser, "Electrochemical boundary conditions for resistance degradation of doped alkaline-earth titanates," *J. Amer. Ceram. Soc.*, vol. 72, no. 12, pp. 2234–2240, Dec. 1989.
- [10] R. Waser, T. Baiatu, and K. H. Härdtl, "DC electrical degradation of perovskite-type titanates: I, ceramics," *J. Amer. Ceram. Soc.*, vol. 73, no. 6, pp. 1645–1653, Jun. 1990.
- [11] R. Waser, T. Baiatu, and K.-H. Härdtl, "DC electrical degradation of perovskite-type titanates: II, single crystals," *J. Amer. Ceram. Soc.*, vol. 73, no. 6, pp. 1654–1662, Jun. 1990.
- [12] T. Baiatu, R. Waser, and K.-H. Härdtl, "DC electrical degradation of perovskite-type titanates: III, a model of the mechanism," *J. Amer. Ceram. Soc.*, vol. 73, no. 6, pp. 1663–1673, Jun. 1990.
- [13] W. Heywang, "Resistivity anomaly in doped barium titanate," *J. Amer. Ceram. Soc.*, vol. 47, no. 10, pp. 484–490, Oct. 1964.
- [14] G. H. Jonker, "Some aspects of semiconducting barium titanate," *Solid-State Electron.*, vol. 7, no. 12, pp. 895–903, Dec. 1964.
- [15] G. H. Jonker, "Halogen treatment of barium titanate semiconductors," *Mater. Res. Bull.*, vol. 2, no. 4, pp. 401–407, Apr. 1967.
- [16] M. Vollman and R. Waser, "Grain boundary defect chemistry of acceptor-doped titanates: Space charge layer width," *J. Amer. Ceram. Soc.*, vol. 77, no. 1, pp. 235–243, Jan. 1994.
- [17] T. Oyama, N. Wada, H. Takagi, and M. Yoshida, "Trapping of oxygen vacancy at grain boundary and its correlation with local atomic configuration and resultant excess energy in barium titanate: A systematic computational analysis," *Phys. Rev. B*, vol. 82, no. 13, pp. 134107–134116, Jul. 2010.
- [18] A. Honda, S. Higai, Y. Motoyoshi, N. Wada, and H. Takagi, "Theoretical study on interactions between oxygen vacancy and doped rare-earth elements in barium titanate," *J. Appl. Phys.*, vol. 50, no. 9, pp. 1143–1146, Oct. 2011.
- [19] H. Moriwake, C. A. J. Fisher, and A. Kuwabara, "First-principles calculations of rare-earth dopants in BaTiO₃," *Jpn. J. Appl. Phys.*, vol. 48, no. 9S1, pp. 09KC031–09KC036, Sep. 2009.
- [20] W. J. Minford, "Accelerated life testing and reliability of high *K* multilayer ceramic capacitors," *IEEE Trans. Compon., Hybrids, Manuf. Technol.*, vol. 5, no. 3, pp. 297–300, Sep. 1982.
- [21] H. Pak and B. Rawal, "Reliability prediction of multilayer ceramic capacitors using an improved accelerated life test and Weibull analysis technique," *Proc. SPIE*, vol. 3235, pp. 362–367, Oct. 1997.
- [22] M. Randall, A. Gurav, D. Skamser, and J. Beeson, "Lifetime modeling of sub 2 micron dielectric thickness BME MLCC," in *Proc. CARTS*, Scottsdale, AZ, USA, Mar. 2003, pp. 134–141.
- [23] J. R. Yoon, K. M. Lee, and S. W. Lee, "Analysis the reliability of multilayer ceramic capacitor with inner Ni electrode under highly accelerated life test conditions," *Trans. Elect. Electron. Mater.*, vol. 10, no. 1, pp. 1229–1234, Feb. 2009.
- [24] M. Cozzolino, "A comparison of BME and traditional technology ceramic capacitors," in *Proc. CARTS*, Orlando, FL, USA, Apr. 2006, pp. 385–394.
- [25] T. Ashburn and D. Skamser, "Highly accelerated testing of capacitors for medical applications," in *Proc. 5th SMTA Med. Electron. Symp.*, Anaheim, CA, USA, Jan. 2008, pp. 124–131.
- [26] J. L. Paulsen and E. K. Reed, "Highly accelerated lifetesting of base-metal-electrode ceramic chip capacitors," *Microelectron. Rel.*, vol. 42, no. 6, pp. 815–820, Jun. 2002.
- [27] D. Liu and M. Sampson, "Reliability evaluation of base-metal-electrode multilayer ceramic capacitors for potential space applications," in *Proc. CARTS*, Jacksonville, FL, USA, Mar. 2011, pp. 45–63.
- [28] D. Liu and M. J. Sampson, "Some aspects of the failure mechanisms in BaTiO₃-based multilayer ceramic capacitors," in *Proc. CARTS*, Las Vegas, NV, USA, Mar. 2012, pp. 59–71.
- [29] D. Liu, "Highly accelerated life stress testing (HALST) of base-metal electrode multilayer ceramic capacitors," in *Proc. CARTS*, Houston, TX, USA, Mar. 2013, pp. 235–248.
- [30] D. Viehland, S. J. Jang, L. E. Cross, and M. Wuttig, "Deviation from Curie-Weiss behavior in relaxor ferroelectrics," *Phys. Rev. B*, vol. 46, no. 13, pp. 8003–8006, Oct. 1992.
- [31] F. A. Kröger and H. J. Vink, "Relations between the concentrations of imperfections in crystalline solids," *Solid State Phys.*, vol. 3, pp. 307–435, Mar. 1956.
- [32] K. A. Connors, *Chemical Kinetics: The Study of Reaction Rates in Solution*. New York, NY, USA: VCH, 1991.
- [33] T. Nakamura, T. Yao, J. Ikeda, N. Kubodera, and H. Takagi, "Improvement of the reliability of dielectrics for MLCC," in *Proc. IOP Conf. Ser., Mater. Sci. Eng.*, vol. 18, no. 9, pp. 092007–092012, 2011.
- [34] E. Brzozowski and M. S. Castro, "Influence of Nb⁵⁺ and Sb³⁺ dopants on the defect profile, PTCR effect and GBBL characteristics of BaTiO₃ ceramics," *J. Eur. Ceram. Soc.*, vol. 24, no. 8, pp. 2499–2507, Jul. 2004.
- [35] T. I. Prokopowicz and A. R. Vaskas, "Research and development intrinsic reliability subminiature ceramic capacitors," Final Report. ECOM-90705-F, 1969 NTIS AD-864068, 1969.
- [36] A. V. Polotai, I. Fujii, D. P. Shay, G.-Y. Yang, E. C. Dickey, and C. A. Randall, "Effect of heating rates during sintering on the electrical properties of ultra-thin Ni-BaTiO₃ multilayer ceramic capacitors," *J. Amer. Ceram. Soc.*, vol. 91, no. 8, pp. 2540–2544, Aug. 2008.
- [37] R. Weachock and D. Liu, "Failure analysis of dielectric breakdowns in base-metal electrode multilayer ceramic capacitors," in *Proc. CARTS*, Houston, TX, USA, Mar. 2013, pp. 151–165.
- [38] J. Illingsworth, H. M. Ai-Allak, and A. W. Brinkman, "Dependence of the grain boundary potential barrier height of BaTiO₃ ceramics on donor dopant concentration," *J. Phys. D, Appl. Phys.*, vol. 23, no. 7, pp. 971–975, Jul. 1990.



Donhang (David) Liu received the Ph.D. degree in electronic engineering from Jiaotong University from a joint Sino-USA education program among Jiaotong University, Pennsylvania State University, and Lehigh University.

He was a Post-Doctoral Research Fellow with the Beckman Institute, University of Illinois at Urbana-Champaign, Champaign, IL, USA, for three years. He joined AVX Corporation, Myrtle Beach, SC, USA, in 1995, as a Principal Engineer and member of technical staff, to develop processing technologies for integrated

passive components with an emphasis on integrated ferroelectrics. In 2000, he began to work with American Technical Ceramics as a Senior RF Engineer for advanced products development. Since 2003, he has supported the NASA Goddard Space Flight Center, Greenbelt, MD, USA, as a Senior Staff Engineer and Senior Staff Engineer II, providing senior level technical supports on space projects. He also serves as a Commodity Expert on capacitor technologies, which includes the evaluation of commercial BME capacitors for aerospace applications. He has authored over 50 technical papers and holds four U.S. patents.